FOR THE RECORD

Two-dimensional crystals of carboxysome shell proteins recapitulate the hexagonal packing of three-dimensional crystals

Kelly A. Dryden,[1] Christopher S. Crowley,[2] Shiho Tanaka,[3] Todd O. Yeates,[2,3]* and Mark Yeager[1,4]*

[1]Department of Molecular Physiology and Biological Physics, University of Virginia Health System, Charlottesville, Virginia 22908

[2]Molecular Biology Institute, University of California, Los Angeles, California 90095

[3]Department of Chemistry and Biochemistry, University of California, Los Angeles, California 90095

[4]Department of Cell Biology, The Scripps Research Institute, La Jolla, California 92037

Received 7 July 2009; Revised 24 September 2009; Accepted 29 September 2009
DOI: 10.1002/pro.272
Published online 20 October 2009 proteinscience.org

Abstract: Bacterial microcompartments (BMCs) are large intracellular bodies that serve as simple organelles in many bacteria. They are proteinaceous structures composed of key enzymes encapsulated by a polyhedral protein shell. In previous studies, the organization of these large shells has been inferred from the conserved packing of the component shell proteins in two-dimensional (2D) layers within the context of three-dimensional (3D) crystals. Here, we show that well-ordered, 2D crystals of carboxysome shell proteins assemble spontaneously when His-tagged proteins bind to a monolayer of nickelated lipid molecules at an air–water interface. The molecular packing within the 2D crystals recapitulates the layered hexagonal sheets observed in 3D crystals. The results reinforce current models for the molecular design of BMC shells.

Keywords: protein assembly; electron microscopy; image analysis; two-dimensional crystallography; carboxysomes; BMC protein

Introduction

Bacterial microcompartments (BMCs) are a family of multisubunit cellular inclusions, dedicated to specific, yet diverse, metabolic functions (for recent reviews, see Refs. 1,2). The operon (Fig. 1a) encodes proteins that assemble as hexamers (Fig. 1b) and form a single-layered outer shell (Fig. 1c,d), which encapsulates several enzymes typically catalyzing sequential metabolic reactions. They function in essence as simple organelles in many bacteria. The shell functions as a selective barrier for molecular access to the microcompartment, thereby enhancing metabolic substrate shunting, while promoting cellular viability by sequestering chemical intermediates that may be either volatile or

Kelly A. Dryden and Christopher S. Crowley contributed equally to this work.

Grant sponsor: NSF; Grant number: MCB-0843065 (TY); Grant sponsor: NIH; Grant number: R01 GM066087 (MY); Grant sponsor: BER Program of the DOE Office of Science (TY).

Correspondence to: Todd O. Yeates, UCLA Department of Chemistry and Biochemistry, 611 Charles Young Dr. East, Los Angeles, CA 90095-1569. E-mail: yeates@mbi.ucla.edu or Mark Yeager, Department of Molecular Physiology and Biological Physics, University of Virginia Health System, 1340 Jefferson Park Avenue, Jordan Hall, Room 4315, Charlottesville, VA 22908-0736. E-mail: yeager@virginia.edu

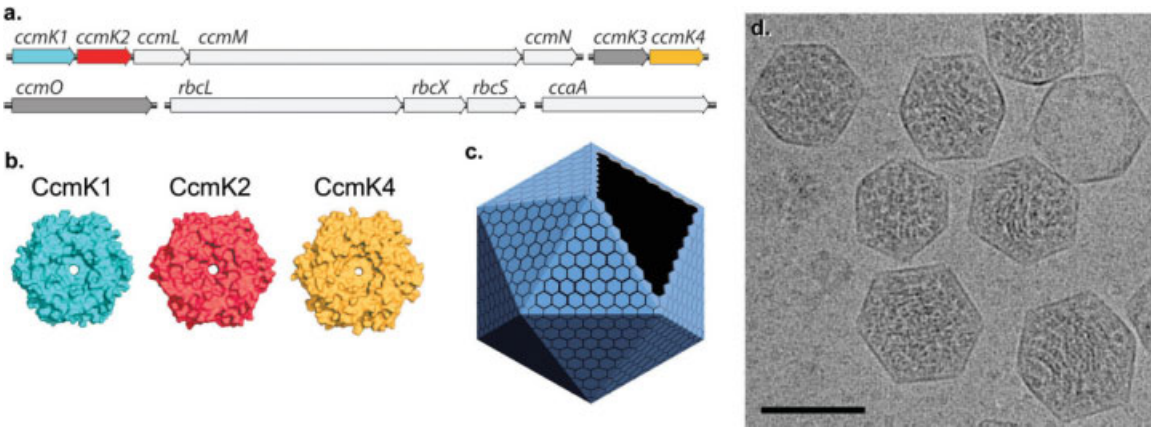

Figure 1. (a) The operon structure for β-carboxysome genes in the cyanobacterium *Synechocystis* PCC 6803. The facets of the carboxysome shell (as shown in c) are believed to be constructed from hexagonal assemblies of the BMC shell protein paralogs, CcmK1, CcmK2, CcmK3, CcmK4, and CcmO. The pentamer vertices are encoded by the gene *ccmL*. The genes *rbcL* and *rbcS* encode the large and small subunits, respectively, of the enzyme RuBisCO, which is localized to the carboxysome interior. Carbonic anhydrase, encoded by the *ccaA* gene, is also located in the carboxysome. *rbcX* encodes a RuBisCO chaperone. *ccmM* and *ccmN* encode additional, non-BMC-type proteins believed to help organize other carboxysome proteins. (b) Surface rendering of the X-ray crystal structures of CcmK1, CcmK2, and CcmK4 hexamers (respective PDB ID codes 3bn4, 3cim, 2a18). Hexamers are the native oligomeric form for all single BMC domain proteins that have been investigated to date. (c) A schematic, idealized depiction of an icosahedral shell of the *Synechocystis* carboxysome. The shell is constructed from tightly packed BMC hexamers forming the facets and CcmL pentamers at the vertices. The diameters of carboxysomes range from 800 to 1400 Å and typically deviate from the perfectly icosahedral symmetry depicted here. (d) Image of intact *Halothiobacillus neapolitanus* carboxysomes recorded by low-dose electron cryomicroscopy. Bar = 100 nm.

toxic to the cell.[3–9] Carboxysomes, which are found in cyanobacteria and some chemoautotrophs, represent prototypical microcompartments. These organelles function as part of the bacterial carbon-concentrating mechanism (CCM) by enhancing the CO_2-fixing RuBisCO reaction, which is notably inefficient.[10–13] Bicarbonate enters bacteria by active transport across the cell membrane and is believed to enter the carboxysome by simple diffusion through the shell. Carboxysomes encapsulate the enzymes carbonic anhydrase (which converts bicarbonate to CO_2) and RuBisCO, thereby providing the latter enzyme with a high luminal concentration of its substrate CO_2, which promotes carbon fixation over the competing oxidase reaction. Recent genomic analyses have revealed several additional types of microcompartments with diverse metabolic functions throughout the eubacteria.[1,14]

Interestingly, diverse types of microcompartments manifest conserved architectural features as revealed by transmission electron microscopy. Within the bacterial cytosol, they appear as faceted, polyhedral electron dense particles, ~1000 Å in diameter. Three-dimensional (3D) reconstructions derived by electron cryotomography showed that the carboxysomes resemble icosahedra,[15,16] though microcompartments of other types appear to be somewhat less geometrically regular.[17] The single-layered shells of microcompartments are formed entirely from protein subunits and lack a lipid bilayer envelope that is typical for vesicular organelles within eukaryotic cells. Each microcompartment shell is typically assembled from a few paralogous protein subunit types, present in a few thousand copies. The major shell proteins of all known BMCs belong to the homologous BMC protein superfamily (conserved domain id cd_6169).

Common features of high-resolution X-ray structures of several BMC proteins illuminate key elements underlying the architecture of the shell and mechanisms of metabolite transport into and out of the microcompartment.[8,18–22] All six of the single BMC domain proteins whose structures have been reported reveal a conserved hexameric assembly having cyclic sixfold symmetry [Fig. 1]. Biophysical methods have confirmed that BMC shell proteins are hexameric in solution,[8,23] supporting the conclusion that hexamers of BMC proteins are the basic building blocks of microcompartment shells. A small pore centered at the sixfold axis has been postulated as a site for diffusion of small molecules across the protein shell.[8] The majority of crystal structures of BMC proteins display tight edge-to-edge packing of hexamers, forming a continuous two-dimensional (2D) molecular sheet in the crystal lattice.[8,20,21] This organization has been hypothesized to represent the packing arrangement of hexamers within the facets of the polyhedral shells forming the microcompartments [Fig. 1(c)]. The close packing of subunits coupled with the central pores within each hexamer provides a mechanism for regulation of molecular diffusion into and out of the shell.

Thus far, the hexagonal 2D sheets of BMC proteins have only been observed in the context of 3D protein crystals, and the purpose of this study was to

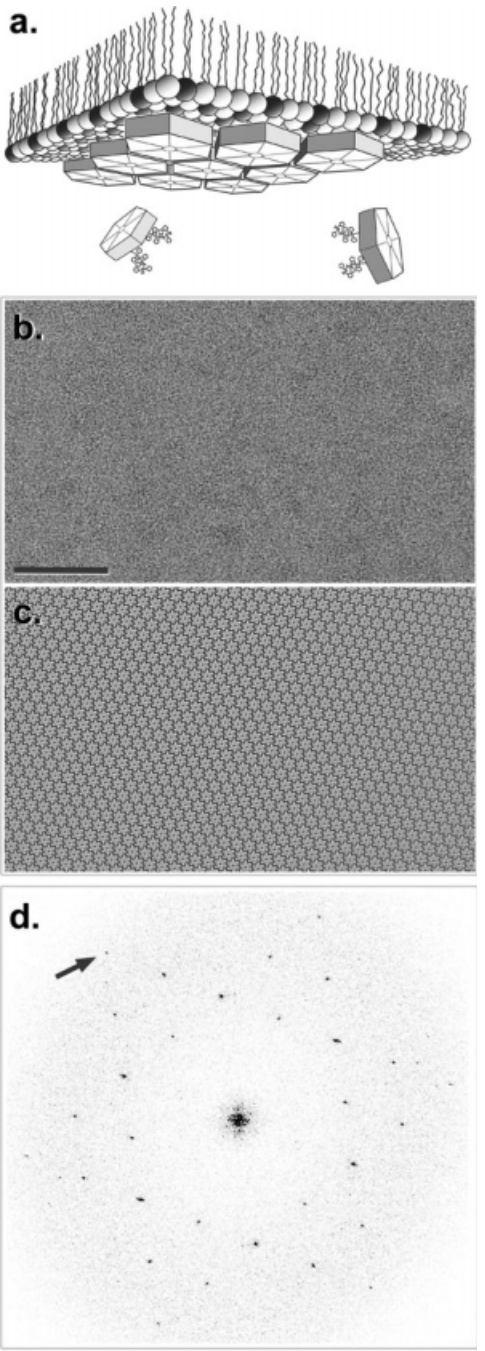

Figure 2. (a) Schematic depiction of 2D lipid monolayer crystallization. Carboxysome BMC shell protein hexamers were localized at the lipid-aqueous interface of a mixed lipid layer with 4:1 (wt:wt) L-α-phosphatidylcholine (light spheres) plus DOGS-NTA-Ni^{2+} (dark spheres) by means of polyhistidine tag chelation via Ni^{2+} bound within the polar lipid layer. Resulting 2D crystals were transferred to an EM grid and stained for image diffraction analysis. (b) Negatively stained TEM image of CcmK1 2D crystals. Scale bar = 100 nm. (c) The underlying order is observed when the image is Fourier filtered, and corrections are made for lattice distortions. (d) The Fourier transform of the negatively stained image displays hexagonal symmetry. The arrow identifies the (2,2) reflection at 17 Å resolution. Images were contrast stretched to emphasize salient features.

determine whether similar lattices could be generated under conditions of 2D crystallization. 2D crystals were formed by the interaction of carboxy-terminally His_6-tagged carboxysome proteins with Ni^{2+}-chelating lipids within monolayers formed at the air–water interface [first described for HIV reverse transcriptase by Kubalek *et al.*,[24] Fig. 2(a)]. From the lipid monolayer, 2D protein crystals were then transferred to carbon-coated grids for electron microscopy (EM) and image analysis. Here, we show that three paralogous carboxysome shell proteins, CcmK1, CcmK2, and CcmK4, form 2D crystals that recapitulate the hexagonal lattice packing observed in previous X-ray crystal structures,[8,20] providing additional evidence that this molecular architecture is the basis for the assembly of the facets within polyhedral BMC shells.

Results and Discussion

Several X-ray crystal structures of BMC shell proteins have displayed 2D hexagonal sheets of hexameric CcmK proteins [Fig. 1(b,c)]. This molecular arrangement is hypothesized to represent the packing of hexamers in the facets of polyhedral carboxysome shells. In the infinite extent, the facets represent 2D hexagonal planes of CcmK hexamers. To test this model, we generated 2D crystals of carboxy-terminally His_6-tagged CcmK1, CcmK2 LM, and CcmK4 using lipid monolayers doped with DOGS-NTA Ni^{2+}-chelating lipids [Fig. 2(a)]. The C-termini reside on one face of the BMC hexamer. As a result, we expect the hexamers to be uniformly oriented with the side bearing the C-terminus facing the lipid layer. Qualitative evaluation of the EM grid area occupied by the sheets suggested that formation of more extensive and well-ordered 2D crystals occurred at higher ionic strength (600 m*M* vs. 300 m*M* NaCl). One of the samples, CcmK2 HM, appeared as nonspecific spheroidal aggregates rather than well-ordered, 2D arrays and was not analyzed further.

Image analysis of negatively stained crystals grown in 600 m*M* NaCl revealed hexagonal lattices with reflections extending to 17 Å for CcmK1 [Fig. 2(b–d)] and 20 Å resolution for CcmK2 LM and CcmK4. The CcmK2 LM and CcmK4 crystals were isomorphous and could be indexed in the plane group p6 with the unit cell dimensions $a = b = 68$ Å (CcmK2) and 70 Å (CcmK4), and $\gamma = 120°$ (both). These values correspond well with the lattice spacings in 3D crystals of CcmK2 LM and CcmK4 [Fig. 3(a)].[8,20] The CcmK2 LM and CcmK4 samples also tended to form multiple, superimposed 2D crystals, which precluded 3D analysis. In comparison with CcmK2 and CcmK4, the CcmK1 crystals were more readily found as monolayers and consistently displayed reflections to slightly higher resolution. These crystals gave p1 unit cell parameters that were nearly hexagonal ($a = 68.2 \pm 0.7$ Å, $b = 69.0 \pm 0.6$ Å, $\gamma = 120.6° \pm 0.7°$, Table I) and in close agreement with the center-to-center spacings

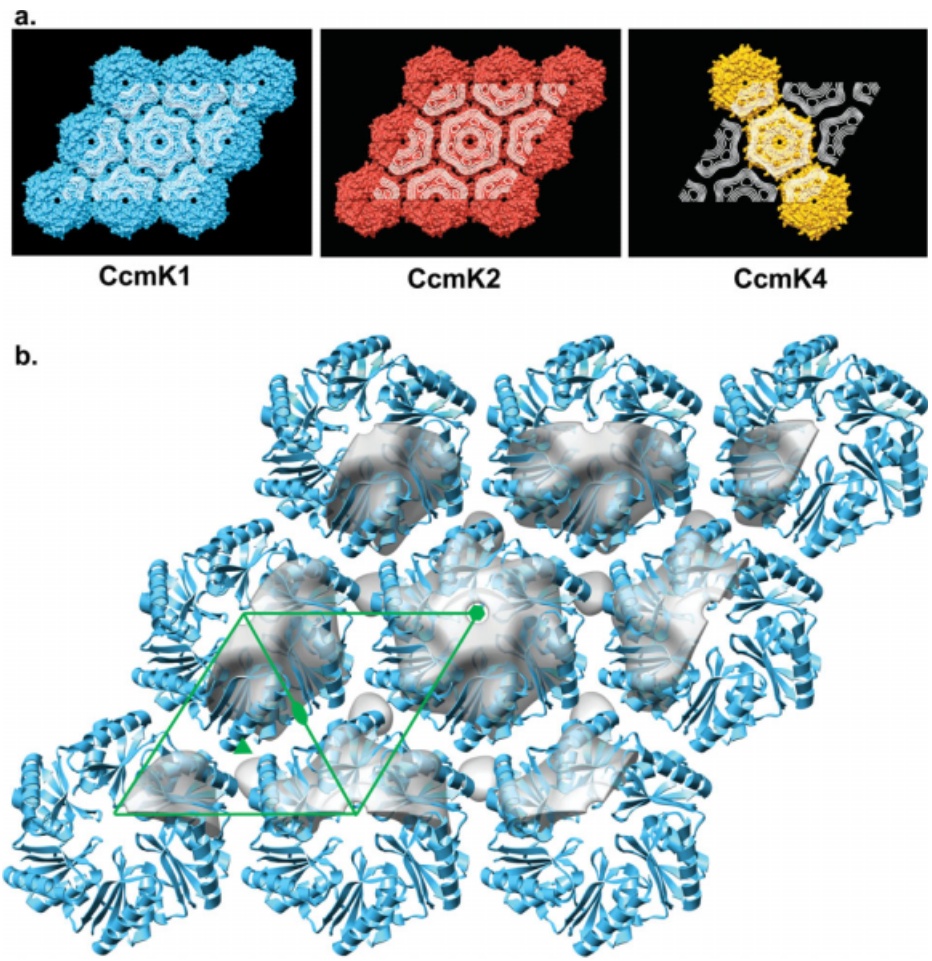

Figure 3. (a) Projection maps from 2D crystals of the three CcmK proteins shown projected onto the molecular packings visualized in 3D crystals. In the case of CcmK4, hexamers in 3D crystals packed into uniformly ordered strips (illustrated), but not uniformly oriented layers. (b) 3D density map (tilted by 15° to enhance depth) showing the hexamer packing of CcmK1 in 2D lipid monolayer crystals (gray surface), which recapitulates the packing in the *ab* lattice plane in 3D crystals (blue ribbon) (pdb id. 3dn9). Center-to-center hexamer spacing is ~68 Å for the EM map and ~70 Å for the crystal structure. For comparison, the X-ray structure was manually docked into the EM density obtained from 3D reconstruction. The green line outlines the 2D unit cell with standard symbols at the axes of rotational symmetry.

in the X-ray structures of CcmK proteins noted earlier [Fig. 3(a,b)].

The reasons for the different qualities of 2D crystals obtained for the three paralogs are unclear, but different BMC paralogs have been noted to exhibit different assembly behaviors.[8,18,20] In particular, 3D crystals of the shell protein CcmK4 displayed linear strips of hexamers rather than uniformly oriented layers.[8] Its lesser tendency to form a uniformly oriented layer was suggested to reflect its lower abundance and potentially special geometric role in the shell. Here, we observe that CcmK4 does form 2D layers of hexamers, which we presume are uniformly oriented owing to the presence of six affinity tags on one side of the hexamer. This could indicate a more permissive assembly behavior than previously indicated. More highly ordered 2D crystals of CcmK4 would be required to show unambiguously whether CcmK4 hexamers pack in a uniformly oriented 2D layer or in alternating strips, as in 3D crystals. We focused further structural analysis on the better diffracting specimens obtained from the CcmK1 shell protein, presumed to be a dominant component of the carboxysome shell.

Assuming p6 symmetry, the merging of data from 28 CcmK1 crystals at tilt angles ranging from 0° to 50° yielded a 3D density map with an in-plane resolution of 18 Å and a *z*-resolution of ~35 Å [Fig. 3(b) and Table I]. Only general interpretations of the EM map are warranted due to the limited resolution. The packing of sixfold symmetric hexamers is in close agreement with the packing of hexamers in the *ab* lattice plane of the CcmK1 3D crystals. In addition, the density for each subunit displays a slight clockwise twist that corresponds fairly well with the subunit ribbon diagram. Similar to the crystal structures of CcmK1, CCmK2, and CcmK4 [Fig. 1(b)], the EM map displays a pore at the center of each hexamer. Density on the threefold axes in the EM map is consistent with tight

Table I. *Statistics of Electron Crystallographic Image Analysis*

2D parameters	
Two-sided plane group	p6
Unit cell parameters	$a = b = 68.5$ Å, $\gamma = 120°$, $c = 90$ Å (arbitrary)
3D reconstruction parameters	
Number of images	28
Range of defocus (μm)	0.45–2.1
IQ cutoff of data	5
Maximum tilt (°)	50.4
Number of observed amplitudes and phases	556[a]
Number of unique reflections	273[b]
In-plane resolution cutoff (Å)	18.0
Estimated resolution normal to plane (Å)	~30
Overall phase residual (°)	15.3[a]
Overall weighted phase residual (°)	9.3[a]

[a] From latfit.com_short.
[b] From merge.com.

packing of adjacent hexamers, such that uranyl salts, which have a grain size of ~15 Å, are excluded in this region. However, we note that the stain-excluding, proteinaceous regions in the EM map (i.e., along the hexamer edges) are smaller than in the ribbon diagram, presumably due to contraction of the protein domains during dehydration of the samples. Aside from deviations attributable to sample preparation and limited resolution, there is general agreement between the EM reconstruction and the packing of CcmK1 subunits observed in 3D crystals.

In summary, EM analysis of 2D crystals supports previous models for the natural assembly of BMC proteins into molecular layers. These layers are believed to form the facets of the polyhedral shell and to regulate diffusion of metabolic substrates and products into and out of BMCs.

Materials and Methods

Sample preparation

The *Synechocystis* PCC 6803 carboxysome proteins CcmK1, CcmK2, and CcmK4 were cloned in the vector pET22b (Novagen, Darmstadt, Germany) for expression of C-terminally His_6-tagged proteins. The proteins were expressed in BL21 (DE3) *E. coli* (Stratagene, La Jolla, CA) and purified following the methods described previously.[8,20] CcmK2 exists as two relatively stable oligomeric species[8] (for clarification, the molecular order of these oligomers is not yet determined). As heterogeneous protein preparations impede crystallization, gel filtration on a Sepharose 75 column (GE Healthcare, Piscataway, NJ) was used to separate the two oligomeric species, hereafter referred to as CcmK2 HM (high molecular weight) and CcmK2 LM (low molecular weight).

Two-dimensional crystallization

Purified protein samples were resuspended in 20 m*M* Tris (pH 7.5), 10 m*M* imidazole, 10% (vol/vol) glycerol, and either 600 m*M* or 300 m*M* NaCl. The protein concentration was adjusted to either 1.0 or 0.5 mg/mL, and then 10 μL of the protein solution was overlaid with 1 μL of a 1:1 chloroform/hexane solution containing 50 mg/mL L-α-phosphatidylcholine doped with 12.5 mg/mL nickel-charged 1,2-dioleoyl-sn-glycero-3-[(*N*-(5-amino-1-carboxypentyl)iminodiacetic acid) succinyl] (DOGS-NTA Ni^{2+}) (Avanti, Alabaster, AL) as previous described.[25] The solutions were incubated in a humid environment for 4 h at room temperature in Teflon-coated wells. The lipid layer was lifted onto glow-discharged continuous-carbon copper grids, rinsed with deionized-distilled water, and negatively stained with 1% uranyl acetate.

Electron microscopy and image analysis

Electron cryomicroscopy of carboxysome samples was performed as previously described for other types of spherical particles.[26,27] 2D crystals of CcmK proteins were analyzed by negative stain EM and image analysis, as previously described[28] (reviewed in Ref. 29). Images were recorded on Kodak SO-163 film using a Tecnai F20 transmission electron microscope (Philips/FEI) operating at 120 kV in low electron-dose mode. Optical diffraction was used to select images with minimal drift and astigmatism, and the negatives were digitized using a Zeiss SCAI densitometer at a step size of 7 mm (corresponding to 1.4 Å on the real image). The images were cropped to 4000 × 4000 or 6000 × 6000 pixels with Adobe Photoshop and converted to the MRC format.[30] The MRC program suite was used to compute Fourier transforms, index the lattices, box the most coherently diffracting areas of each crystal, and correct for lattice distortions and effects of the contrast transfer function (CTF).[30] The program ALLSPACE[31] was used to determine the 2D plane group symmetry and calculate the appropriate phase origins used for image alignment. The best image recorded from an untilted CcmK1 sample was used as

a reference to determine the phase origin of the remaining images. Lattice lines were then fitted to the 3D data, and an initial map was created using the CCP4 suite of programs.[32] The phase origins and tilt geometries of each crystal were then refined against this initial model. Iterative refinements of the tilt geometry and CTF corrections against subsequent models were continued until there was no further improvement in the overall phase residual. After obtaining the most self-consistent set of image parameters, the data set was again remerged and averaged, lattice lines were fitted, and a final 3D map was generated by Fourier inversion.

Acknowledgments

The authors thank Barbie Ganser-Pornillos for technical assistance with image processing. Purified *Halothiobacillus neapolitanus* carboxysomes were generously provided by Prof. Gordon C. Cannon and Prof. Sabine Heinhorst (University of Southern Mississippi, Hattiesburg, MS 39406-0001).

References

1. Yeates TO, Kerfeld CA, Heinhorst S, Cannon GC, Shively JM (2008) Protein-based organelles in bacteria: carboxysomes and related microcompartments. Nat Rev Microbiol 6:681–691.
2. Cheng S, Liu Y, Crowley CS, Yeates TO, Bobik TA (2008) Bacterial microcompartments: their properties and paradoxes. Bioessays 30:1084–1095.
3. Sampson EM, Bobik TA (2008) Microcompartments for B_{12}-dependent 1,2-propanediol degradation provide protection from DNA and cellular damage by a reactive metabolic intermediate. J Bacteriol 190:2966–2971.
4. Penrod JT, Roth JR (2006) Conserving a volatile metabolite: a role for carboxysome-like organelles in *Salmonella enterica*. J Bacteriol 188:2865–2874.
5. Brinsmade SR, Paldon T, Escalante-Semerena JC (2005) Minimal functions and physiological conditions required for growth of *Salmonella enterica* on ethanolamine in the absence of the metabolosome. J Bacteriol 187: 8039–8046.
6. Rondon MR, Kazmierczak R, Escalante-Semerena JC (1995) Glutathione is required for maximal transcription of the cobalamin biosynthetic and 1,2-propanediol utilization (*cob/pdu*) regulon and for the catabolism of ethanolamine, 1,2-propanediol, and propionate in *Salmonella typhimurium* LT2. J Bacteriol 177:5434–5439.
7. Havemann GD, Sampson EM, Bobik TA (2002) PduA is a shell protein of polyhedral organelles involved in coenzyme B_{12}-dependent degradation of 1,2-propanediol in *Salmonella enterica* serovar typhimurium LT2. J Bacteriol 184:1253–1261.
8. Kerfeld CA, Sawaya MR, Tanaka S, Nguyen CV, Phillips M, Beeby M, Yeates TO (2005) Protein structures forming the shell of primitive bacterial organelles. Science 309:936–938.
9. Stojiljkovic I, Bäumler AJ, Heffron F (1995) Ethanolamine utilization in *Salmonella typhimurium*: nucleotide sequence, protein expression, and mutational analysis of the cchA cchB eutE eutJ eutG eutH gene cluster. J Bacteriol 177:1357–1366.
10. Badger MR, Price GD (2003) CO_2 concentrating mechanisms in cyanobacteria: molecular components, their diversity and evolution. J Exp Bot 54:609–622.
11. Badger MR, Price GD, Long BM, Woodger FJ (2006) The environmental plasticity and ecological genomics of the cyanobacterial CO_2 concentrating mechanism. J Exp Bot 57:249–265.
12. Cannon GC, Bradburne CE, Aldrich HC, Baker SH, Heinhorst S, Shively JM (2001) Microcompartments in prokaryotes: carboxysomes and related polyhedra. Appl Environ Microbiol 67:5351–5361.
13. Shively JM, English RS, Baker SH, Cannon GC (2001) Carbon cycling: the prokaryotic contribution. Curr Opin Microbiol 4:301–306.
14. Bobik TA (2006) Polyhedral organelles compartmenting bacterial metabolic processes. Appl Microbiol Biotechnol 70:517–525.
15. Iancu CV, Ding HJ, Morris DM, Dias DP, Gonzales AD, Martino A, Jensen GJ (2007) The structure of isolated *Synechococcus* strain WH8102 carboxysomes as revealed by electron cryotomography. J Mol Biol 372:764–773.
16. Schmid MF, Paredes AM, Khant HA, Soyer F, Aldrich HC, Chiu W, Shively JM (2006) Structure of *Halothiobacillus neapolitanus* carboxysomes by cryo-electron tomography. J Mol Biol 364:526–535.
17. Bobik TA, Havemann GD, Busch RJ, Williams DS, Aldrich HC (1999) The propanediol utilization (pdu) operon of *Salmonella enterica* serovar typhimurium LT2 includes genes necessary for formation of polyhedral organelles involved in coenzyme B_{12}-dependent 1,2-propanediol degradation. J Bacteriol 181:5967–5975.
18. Crowley CS, Sawaya MR, Bobik TA, Yeates TO (2008) Structure of the PduU shell protein from the Pdu microcompartment of *Salmonella*. Structure 16:1324–1332.
19. Klein MG, Zwart P, Bagby SC, Cai F, Chisholm SW, Heinhorst S, Cannon GC, Kerfeld CA (2009) Identification and structural analysis of a novel carboxysome shell protein with implications for metabolite transport. J Mol Biol 392:319–333.
20. Tanaka S, Kerfeld CA, Sawaya MR, Cai F, Heinhorst S, Cannon GC, Yeates TO (2008) Atomic-level models of the bacterial carboxysome shell. Science 319:1083–1086.
21. Tsai Y, Sawaya MR, Cannon GC, Cai F, Williams EB, Heinhorst S, Kerfeld CA, Yeates TO (2007) Structural analysis of CsoS1A and the protein shell of the *Halothiobacillus neapolitanus* carboxysome. PLoS Biol 5: 1345–1354.
22. Sagermann M, Ohtaki A, Nikolakakis K (2009) Crystal structure of the EutL shell protein of the ethanolamine ammonia lyase microcompartment. Proc Natl Acad Sci USA 106:8883–8887.
23. Tanaka S, Sawaya MR, Phillips M, Yeates TO (2009) Insights from multiple structures of the shell proteins from the β-carboxysome. Protein Sci 18:108–120.
24. Kubalek EW, Le Grice SFJ, Brown PO (1994) Two-dimensional crystallization of histidine-tagged, HIV-1 reverse transcriptase promoted by a novel nickel-chelating lipid. J Struct Biol 113:117–123.
25. Barklis E, McDermott J, Wilkens S, Schabtach E, Schmid MF, Fuller S, Karanjia S, Love Z, Jones R, Rui Y, Zhao X, Thompson D (1997) Structural analysis of membrane-bound retrovirus capsid proteins. EMBO J 16:1199–1213.
26. Tihova M, Dryden KA, Le TL, Harvey SC, Johnson JE, Yeager M, Schneemann A (2004) Nodavirus coat protein imposes dodecahedral RNA structure independent of nucleotide sequence and length. J Virol 78:2897–2905.

27. Dryden KA, Wieland SF, Whitten-Bauer C, Gerin JL, Chisari FV, Yeager M (2006) Native hepatitis B virions and capsids visualized by electron cryomicroscopy. Mol Cell 22:843–850.
28. Ganser BK, Cheng A, Sundquist WI, Yeager M (2003) Three-dimensional structure of the M-MuLV CA protein on a lipid monolayer: a general model for retroviral capsid assembly. EMBO J 22:2886–2892.
29. Yeager M, Unger VM, Mitra AK (1999) Three-dimensional structure of membrane proteins determined by two-dimensional crystallization, electron cryomicroscopy, and image analysis. Methods Enzymol 294:135–180.
30. Crowther RA, Henderson R, Smith JM (1996) MRC image processing programs. J Struct Biol 116:9–16.
31. Valpuesta JM, Carrascosa JL, Henderson R (1994) Analysis of electron microscope images and electron diffraction patterns of thin crystals of ϕ29 connectors in ice. J Mol Biol 240:281–287.
32. CCP4 (1994) The CCP4 suite: programs for protein crystallography. Acta Crystallogr D Biol Crystallogr 50:760–763.